Active Contours without Edges and Curvature Analysis for Endoscopic Image Classification

B. V. Dhandra dhandra_b_v@yahoo.co.in
Dept. of Computer Science
Gulbarga University
Gulbarga - 585106, INDIA.

Ravindra Hegadi ravindrahegadi@rediffmail.com
Dept. of Computer Science
Gulbarga University
Gulbarga - 585106, INDIA.

Abstract

Endoscopic images do not contain sharp edges to segment using the traditional segmentation methods for obtaining edges. Therefore, the active contours or 'snakes' using level set method with the energy minimization algorithm is adopted here to segment these images. The results obtained from the above segmentation process will be number of segmented regions. The boundary of each region is considered as a curve for further processing. The curvature for each point of this curve is computed considering the support region of each point. The possible presence of abnormality is identified, when curvature of the contour segment between two zero crossings has the opposite curvature signs to those of such neighboring contour segments on the same edge contours. The K-nearest neighbor classifier is used to classify the images as normal or abnormal. The experiment based on the proposed method is carried out on 50 normal and 50 abnormal endoscopic images and the results are encouraging.

Keywords: Active Contours, Curvature, Endoscopy, Jacobi method, Level sets.

1. INTRODUCTION

Endoscopy provides images better than that of the other tests, and in many cases endoscopy is superior to the other imaging techniques such as traditional x-rays. A physician may use an endoscopy as a tool for diagnosing the possible disorders in the digestive tract. Symptoms that may indicate the need for an endoscopy include swallowing difficulties, nausea, vomiting, reflux, bleeding, indigestion, abdominal pain, chest pain and a change in bowel habits. In the conventional approach for the diagnosis of endoscopic images the visual interpretation by the physician is employed. The process of computerized visualization, interpretation and analysis of endoscopic images will assist the physician for fast identification of the abnormality in the images [1]. In this direction research works are being carried out for classifying the abnormal endoscopic images based on their properties like color, texture, structural relationships between the image pixels, etc. The method proposed by P.Wang et.al.[2] classifies the endoscopic images based on texture and neural network, where as the analysis of curvature for the edges obtained from the endoscopic images is proposed by Krishnan et.al.[3]. Hiremath et.al.[4] proposed a method to detect the possible presence of abnormality using color segmentation of the images based on 3σ-

interval [5] for obtaining edges followed by curvature analysis. The watershed segmentation approach for classifying abnormal endoscopic images is proposed by Dhandra et.al.[6]. In this paper the active contours using the level set method with energy minimization approach, which is also known as active contours without edges proposed by chan et.al [7] is adopted for the segmentation of the endoscopic images followed by the curvature computation of the boundary of each obtained region. The zero crossings of the curvature plot for each edge are obtained for further analysis. In the following section we shall discuss the mathematical formulation for level set method and active contours without edges. In Section 3 the curvature analysis is discussed. In Section 4 the K nearest neighborhood classification is discussed. The experimental results are analyzed in Section 5.

2. METHODS

2.1 Mathematical formulations for Level Set Method

Let Ω be a bounded open subset of R^2, with $\partial\Omega$ as its boundary. Then a two dimensional image u_0 can be defined as $u_0 : \Omega \rightarrow R$. In this case Ω is just a fixed rectangular grid. Now consider the evolving curve C in Ω, as the boundary of an open subset ω of Ω. In other words, $\omega \subseteq \Omega$, and C is the boundary of ω $(C = \partial\omega)$. The main idea is to embed this propagating curve as the zero level set of a higher dimensional function ϕ . We define the function as follows:

$$\varphi(x,y,t=0) = \pm d \tag{1}$$

where d is the distance from (x, y) to $\partial\omega$ at $t = 0$, and the plus (minus) sign is chosen if the point (x, y) is outside (inside) the subset ω.

Now, the goal is to obtain an equation for the evolution of the curve. Evolving the curve in the direction of its normal amounts to solving the partial differential equation [8]:

$$\frac{\partial\phi}{\partial t} = F|\nabla\phi|,\ \phi(x,y,t=0) = \phi_0(x,y),$$

where the set $\{(x,y), \phi_0(x,y) = 0\}$ defines the initial contour, and F is the speed of propagation. For certain forms of the speed function, F, the above equation reduces to a standard Hamilton-Jacobi equation. There are several major advantages to this formulation. The first one is that $\phi(x,y,t)$ always remains a function as long as F is smooth. As the surface ϕ evolves, the curve C may break, merge, and change topology. Second advantage is that geometric properties of the curve are easily determined from a particular level set of the surface ϕ . For example, the normal vector for any point on the curve C is given by:

$$\vec{h} = \nabla\phi$$

and curvature K is obtained from the divergence of the gradient of unit normal vector to the front:

$$K = div\left(\frac{\nabla\phi}{|\nabla\phi|}\right) = \frac{\phi_{xx}\phi_y^2 - 2\phi_x\phi_y\phi_{xy} + \phi_{yy}\phi_x^2}{\left(\phi_x^2 + \phi_y^2\right)^{3/2}}$$

The third advantage is that we are able to evolve curves in more than two dimensions. The above formulae can easily be extended for higher dimensions. This is useful in propagating a curve to segment large volume of data.

2.2 Active Contours using level set method without edges

The curve *C* can be considered as the boundary of the *ω* and the region *ω* can be denoted by *inside(C)* and the region $\Omega \setminus \overline{\omega}$ by *outside(C)*. The energy minimization approach proposed by Chan et.al.[7] is adopted for segmentation is as follows:

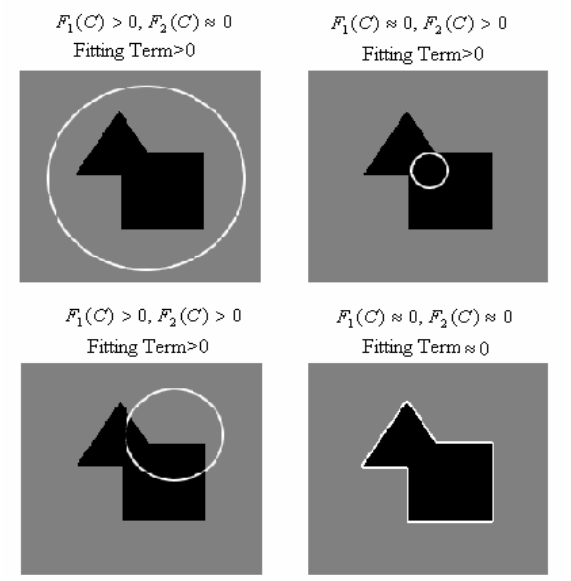

FIGURE 1: All possible cases in position of the curve

Consider a simple case where the image u_0 is formed by two regions of piecewise constant intensity. Denote the intensity values by u_0^0 and u_0^1. Further, assume that the object to be detected has a region whose boundary is C_0 and intensity u_0^1. Then *inside(C₀),* the intensity of u_0 is approximately u_0^1, whereas *outside(C₀)* the intensity of u_0 is approximately u_0^0. Then consider the fitting term:

$$F_1(C) + F_2(C) = \int_{inside(c)} \left|u_0(x,y) - c_1\right|^2 dxdy + \int_{outside(c)} \left|u_0(x,y) - c_2\right|^2 dxdy$$

where the constants c_1 and c_2 are the averages of u_0 inside and outside the curve *C* respectively.

Consider Fig. 1. If the curve *C* is outside the object, then $F_1(C) > 0, F_2(C) \approx 0$. If the curve is inside the object, then $F_1(C) \approx 0, F_2(C) > 0$. If the curve is both inside and outside the object, then $F_1(C) > 0, F_2(C) > 0$. However, if the curve *C* is exactly on our object boundary C_0, then $F_1(C) \approx 0, F_2(C) \approx 0$, and our fitting term is minimized.

Some additional regularization terms of Mumford-Shah segmentation model [9] are considered for effective energy minimization. Therefore we will also try to minimize the length of the curve and the area of the region inside the curve. So we introduce the energy function *E*:

$$E(C, c_1, c_2) = \mu \cdot length(C) + \nu \cdot Area(inside(C)) + \lambda_1 \cdot \int_{inside(c)} \left|u_0(x,y) - c_1\right|^2 dxdy + \lambda_2 \cdot \int_{outside(c)} \left|u_0(x,y) - c_2\right|^2 dxdy$$

where $\mu \geq 0, \nu \geq 0, \lambda_1 > 0, \lambda_2 > 0$ are fixed parameters. Thus, the objective is to find *C, c_1, c_2* such that *E(C, c_1, c_2)* is minimized. Mathematically, solve:

$$\inf_{C, c_1, c_2} E(C, c_1, c_2)$$

This problem can be formulated using level set method as follows. The evolving curve *C* can be represented by the zero level set of the signed distance function ϕ as in (1). So we replace the unknown variable *C* by ϕ. Now consider the Heaviside function *H* and Dirac measure *δ*:

$$H(z) = \begin{cases} 1, \ if \ \ z \geq 0 \\ 0, \ if \ \ z < 0 \end{cases}, \qquad \delta(z) = \frac{d}{dz} H(z)$$

We can rewrite the length of ϕ *= 0* and the area of the region *inside(ϕ = 0)* using these functions. The Heaviside function is positive inside our curve and zero elsewhere, so the area of the region is just the integral of the Heaviside function of ϕ. The gradient of the Heaviside function defines our curve, so integrating over this region gives the length of the curve. Mathematically:

$$Area(\phi = 0) = \int_\Omega H(\phi(x, y))dxdy$$

$$Length(\phi = 0) = \int_\Omega \left|\nabla H(\phi(x, y))\right| dxdy = \int_\Omega \delta(\phi(x, y)) \left|\nabla \phi(x, y)\right| dxdy$$

Similarly, we can rewrite the previous energy equations so that they are defined over the entire domain Ω rather than separated into *inside(C) =ϕ > 0* and *outside(C) = ϕ < 0*:

$$\int_{\phi>0} \left|u_0(x, y) - c_1\right|^2 dxdy = \int_\Omega \left|u_0(x, y) - c_1\right|^2 H(\phi(x, y))dxdy$$

$$\int_{\phi<0} \left|u_0(x, y) - c_2\right|^2 dxdy = \int_\Omega \left|u_0(x, y) - c_2\right|^2 (1 - H(\phi(x, y)))dxdy$$

Therefore our energy function *E(C,c_1,ϕ)* can be written as:

$$\begin{aligned} E(C, c_1, c_2) = {} & \mu \int_\Omega \delta(\phi(x, y)) \left|\nabla \phi(x, y)\right| dxdy + \nu \int_\Omega H(\phi(x, y))dxdy \\ & + \lambda_1 \int_\Omega \left|u_0(x, y) - c_1\right|^2 H(\phi(x, y))dxdy \\ & + \lambda_2 \int_\Omega \left|u_0(x, y) - c_2\right|^2 (1 - H(\phi(x, y)))dxdy \end{aligned} \qquad (2)$$

The constants c_1, c_2 are the averages of u_0 in $\phi \geq 0$ and $\phi < 0$ respectively. So they are easily computed as:

$$c_1(\phi) = \frac{\int_\Omega u_0(x, y) H(\phi(x, y))dxdy}{\int_\Omega H(\phi(x, y))dxdy} \qquad (3)$$

and

$$c_2(\phi) = \frac{\int_\Omega u_0(x,y)(1 - H(\phi(x,y)))dxdy}{\int_\Omega (1 - H(\phi(x,y)))dxdy} \tag{4}$$

Now we can deduce the Euler-Lagrange partial differential equation from (2). We parameterize the descent direction by $t \geq 0$, so the equation $\phi(x, y, t)$ is:

$$\frac{\partial \phi}{\partial t} = \partial(\phi)\left[\mu\, div\left(\frac{\nabla\phi}{|\nabla\phi|}\right) - \nu - \lambda_1(u_0 - c_1)^2 + \lambda_2(u_0 - c_2)^2\right] = 0 \tag{5}$$

In order to solve this partial differential equation, we first need to regularize *H(z)* and *δ(z)*. Chan and Vese [7] propose:

$$H_\varepsilon(z) = \frac{1}{2} + \frac{1}{\pi}\arctan\left(\frac{z}{\varepsilon}\right)$$

Implying that *δ(z)* regularizes to:

$$\delta_\varepsilon(z) = \frac{1}{\pi}\cdot\frac{\varepsilon}{\varepsilon^2 + z^2}$$

It is easy to see that as $\varepsilon \to 0$, $H_\varepsilon(z)$ converges to *H(z)* and $\delta_\varepsilon(z)$ converges to $\delta(z)$. Authors claim that with these regularizations, the algorithm has the tendency to compute a global minimizer. Chan and Vese [7] give the following discretization and linearization of (5):

$$\begin{aligned}\frac{\phi_{i,j}^{n+1} - \phi_{i,j}^n}{\Delta t} = \delta_\varepsilon\left(\phi_{i,j}^n\right)\Bigg[&\frac{\mu}{h^2}\Delta_-^x \cdot \left(\frac{\Delta_+^x \phi_{i,j}^{n+1}}{\sqrt{\left(\Delta_+^x \phi_{i,j}^n\right)^2/(h^{2)} + \left(\phi_{i,j+1}^n - \phi_{i,j-1}^n\right)^2/(2h)^2}}\right) \\ &+ \frac{\mu}{h^2}\Delta_-^y \cdot \left(\frac{\Delta_+^y \phi_{i,j}^{n+1}}{\sqrt{\left(\phi_{i+1,j}^n - \phi_{i-1,j}^n\right)^2/(2h)^2 + \left(\Delta_+^y \phi_{i,j}^n\right)^2/(h^2)}}\right) \\ &- \nu - \lambda_1\left(u_{0,i,j} - c_1(\phi^n)\right)^2 + \lambda_2\left(u_{0,i,j} - c_2(\phi^n)\right)^2\Bigg]\end{aligned} \tag{6}$$

where the forward differences of $\phi_{i,j}^n$ are calculated as:

$$\Delta_-^x \phi_{i,j} = \phi_{i,j} - \phi_{i-1,j}, \quad \Delta_+^x \phi_{i,j} = \phi_{i+1,j} - \phi_{i,j},$$
$$\Delta_-^y \phi_{i,j} = \phi_{i,j} - \phi_{i,j-1}, \quad \Delta_+^y \phi_{i,j} = \phi_{i,j-1} - \phi_{i,j}$$

This linear system also depends on the forward differences of $\phi_{i,j}^{n+1}$, which is an unknown. However these can be solved using the Jacobi method [10]. In practice, the number of iterations until convergence was found to be small. The segmentation algorithm is then given by:

1. **Initialize** ϕ^0 by ϕ_0, *n=0*
2. **For** *fixed number of iterations* **do**
   - **2.1 Compute** $c_1(\phi^n)$ and $c_2(\phi^n)$ using (3) and (4)
   - **2.2 Estimate** forward differences of ϕ^{n+1} using Jacobi method
   - **2.3 Compute** ϕ^{n+1} using (6)
3. **End.**

ALGORITHM 1: Energy minimization with Jacobi method.

3. CURVATURE COMPUTATION

The result of the method proposed in Section 2 will generate a number of regions. The boundary of each region is considered for the curvature computation. Due to the discrete boundary representation and quantization errors, false local concavities and convexities along a contour are formed. This noisy nature of binary contours must be taken into account to obtain reliable estimates of contour curvature. Hence, a Gaussian filter is used to smooth the contour points to reduce the noise effect [11]. However, the width of Gaussian filter, *w*, that controls the degree of smoothing has to be chosen suitably. A large value of *w* will remove all small details of the contour curvature, while a small value will permit false concavities and convexities to remain in the contour, thus enforcing an appropriate choice of *w*. To overcome this problem a support region is employed which will dynamically determine the parameter of the Gaussian filter.

3.1 Determination of Support Region

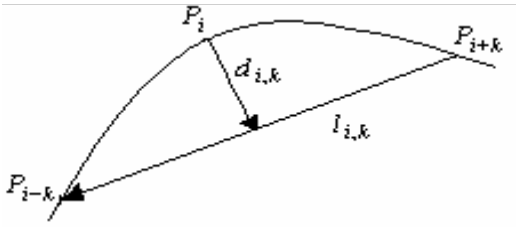

FIGURE 2: Representation of Support Region.

The support region concept can be explained using the Fig. 2. The support region for each point on the curve is the number of points obtained from the implementation of the Algorithm 2:

1. *Determine the length of the chord joining the points* P_{i-k}, P_{i+k} *as*

$$l_{i,k} = \left| \overline{P_{i-k} P_{i+k}} \right|$$

2. *Let* $d_{i,k}$ *be the perpendicular distance from* P_i *to the line joining* $\overline{P_{i-k} P_{i+k}}$ *, start with k=1, compute* $l_{i,k}$ *and* $d_{i,k}$ *until one of the following conditions hold:*

   a. $l_{i,k} \geq l_{i,k+1}$

   b. $\frac{\mathrm{d_{i,k}}}{\mathrm{l_{i,k}}} \geq \frac{d_{i,k+1}}{l_{i,k+1}}$ *for* $d_{i,k} \geq 0$

3. *Now, the region of support of* P_i *is the set of points satisfying either condition (a) or condition (b), that is,*

$$D(P_i) = \{P_{i-k}, ..., P_{i-1}, P_i, P_{i+1}, ..., P_{i+k} \mid condition\ (a)\ or\ (b)\}$$

ALGORITHM 2: Determination of support region

3.2 Gaussian Smoothing

A planar curve can be defined in parametric form as $(x(t), y(t)) \in R^2$, where t is the path length along the curve. Smoothing is performed by the convolution of $x(t)$ and $y(t)$ with the Gaussian filter. A one dimensional Gaussian filter is defined as

$$\eta(t, w) = \frac{1}{\sqrt{2\pi w^2}} e^{\left(-t^2/2w^2\right)}$$

where w is the width of the filter, which needs to be determined. The smoothed curve is denoted by set of points $(X(t,w), Y(t,w))$, where,

$$x(t, w) = x(t) \otimes \eta(t, w), \quad y(t, w) = y(t) \otimes \eta(t, w)$$

where $\otimes$ denotes the convolution.

The measurement of the curvature of the point is based on the local properties within its region of support, and the length of Gaussian smooth filter is proportional to the region of support [12]. This implies that the neighboring points closer to the point of interest should have higher weights than those points further away. This method is less sensitive to noise. The Gaussian filter applied here will have the following window length and width [3]:

Window Len =2xSupp. Region $D(P_i)$+1,
Width w =Support Region $D(P_i)$ / 3

Further, the curvature for each point on the curve is calculated in the following way.

3.3 Curvature Computation

For the continuous curve C, expressed by $\{x(s), y(s)\}$, where s is the arc length of the edge point, the curvature can be expressed as:

$$k(s) = \frac{\dot{x}\ddot{y} - \ddot{x}\dot{y}}{\left(\dot{x}^2 + \dot{y}^2\right)^{3/2}} \tag{7}$$

where $\dot{x} = dx/ds$, $\ddot{x} = d^2x/ds^2$, $\dot{y} = dy/ds$, $\ddot{y} = d^2y/ds^2$.

For digital implementation, the coordinate functions $x(s)$ and $y(s)$ of the curvature are represented by a set of equally spaced Cartesian grid samples. The derivatives in the equation (7) are calculated by finite differences as:

$$\begin{aligned} \dot{x}_i &= x_i - x_{i-1}, \ \ddot{x}_i = x_{i-1} - 2x_i + x_{i+1}, \\ \dot{y}_i &= y_i - y_{i-1}, \ \ddot{y}_i = y_{i-1} - 2y_i + y_{i+1} \end{aligned} \tag{8}$$

The algorithm for curvature computation is presented below.

1. *Determine edge contours in the input image using active contours without edges.*
2. *Select a large edge contour for further processing.*
3. *Determine the support region for each contour point.*
4. *Smooth the contour by a Gaussian filter with the width proportional to the support region.*

5. *Compute the curvature for each point on the Gaussian smoothed curve using equation (7) and (8).*

ALGORITHM 3: Curvature computation

In the process of curvature computation we come across with two special conditions for which the alternate solutions need to be given. They are:

1. When the edge point is on a straight line, the curvature for that point is assigned to zero.
2. When the support region for an edge point is 1, this point will not be smoothed. So, the smoothing on this point is performed using the following equation:

$$(\overline{x}_{i,}\overline{y}_{i})=\frac{1}{2}(x_i,y_i)+\frac{1}{4}[(x_{i-1},y_{i-1})+(x_{i+1},y_{i+1})]$$

where, $(\overline{x}_{i,}\overline{y}_{i})$ is the smoothed point of (x_i,y_i).

4. K-NEAREST NEIGHBOR CLASSIFIER

The nearest neighbor and K-nearest neighbor classifiers are applied on two parameters namely the number of regions obtained from the segmentation process and the total number of zero crossings of curvature plot of every region edge to classify the images as either normal or abnormal. Basically this classifier finds the closest training point to the unknown point and predicts the category of that training point for this unknown point. The experiment is carried out by varying the number of neighbors (K=3, 5, 7). Performance of the algorithm is optimal when K=3.

5. EXPERIMENTAL RESULTS

For the experimentation 50 normal and 50 abnormal endoscopic color images of size 128X128 pixels are chosen. The parameters are set to the values as: $\lambda_1=\lambda_2=1$, *h =1*, and $\Delta t=0.1$. Varying the value of ν generally had little or no effect on the segmentation results. The ε parameter for the regularized Heaviside and Dirac functions was set to 1 as suggested by Chan and Vese [7]. The length parameter μ is fixed to a small value (i.e. $\mu\approx 0.0001\cdot 255^2$).The detection of possible presence of abnormality is performed by analyzing the curvature change along boundary of each region, which is considered as a edge contour. The curvature of each edge point on the edge contour is computed using the Algorithm 3. Two thresholds, c_{th} and $n_{th,}$ are used in the analysis. c_{th} is the curvature threshold value, and n_{th} is number of edge points in a segment. Along the edge contour, if the absolute curvature of the point is bigger than c_{th}, the point counting starts until the absolute curvature value of the point is less than c_{th}. If the point count is bigger than n_{th}, an edge segment is formed. The possible presence of abnormality in the image is detected when the curvature of a segment has opposite sign to those of such neighboring segments on the same edge contour. Also such a segment is bounded by two significant zero crossings. The stages in the proposed method for the abnormal images and normal images are shown in the Fig. 3 and 4 respectively. In these figures image [A] is abnormal endoscopic color image, [B] shows regions obtained after the segmentation of images using active contours without edges. Its binary image is shown in image [C]. A largest edge contour obtained is shown in image [D]. Its curvature profile is shown in image [E]. In the abnormal image shown in Fig. 3, the number of regions formed is 12, and the number of zero crossings obtained for a large edge contour is 137, where as for the normal image shown in Fig. 4, the number of regions formed is 5, and the number of zero crossings obtained for a large edge contour is 24. Fig. 5 and Fig. 6 show the endoscopic images with their curvature plot for their largest edges. The original abnormal and normal endoscopic images are shown in the first column and the corresponding curvature profile for the largest edge segment is shown in the second column. From these figures, considerably

less number of zero crossings for the normal image edge curvatures can be observed as opposed to the number of zero crossings of edge curvatures in the abnormal images.

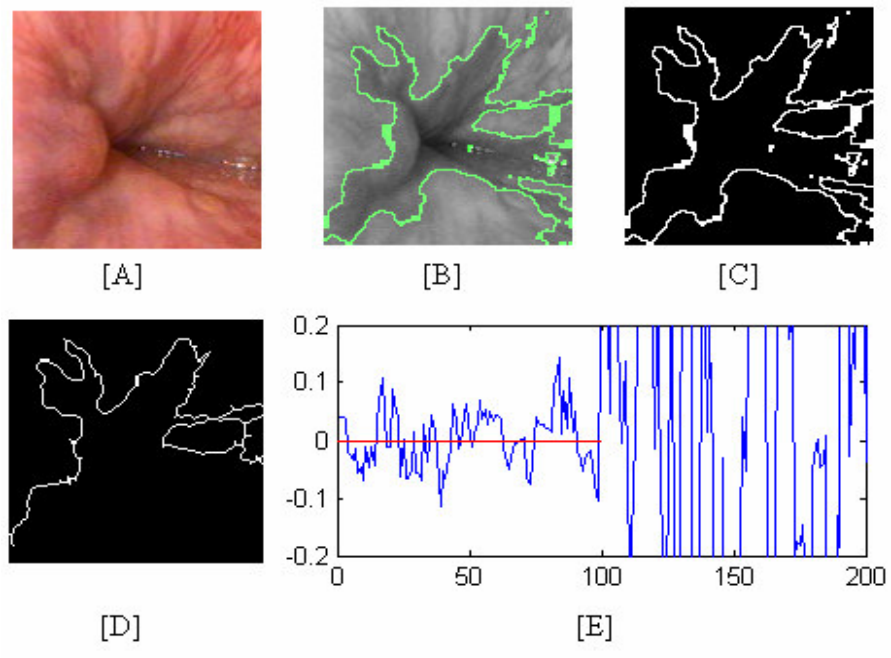

FIGURE 3: The proposed method for Abnormal Image.

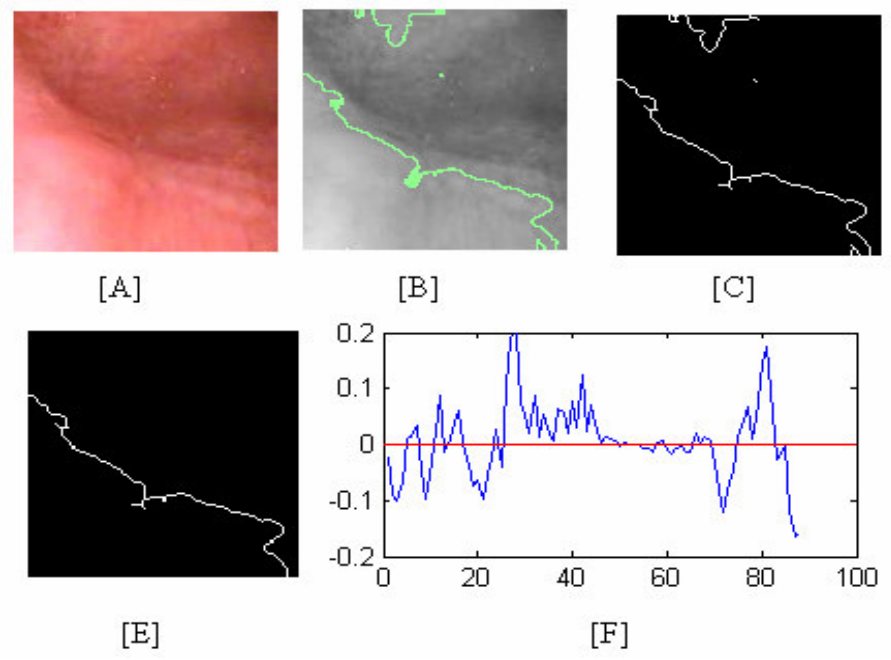

FIGURE 4: The proposed method for Normal Images.

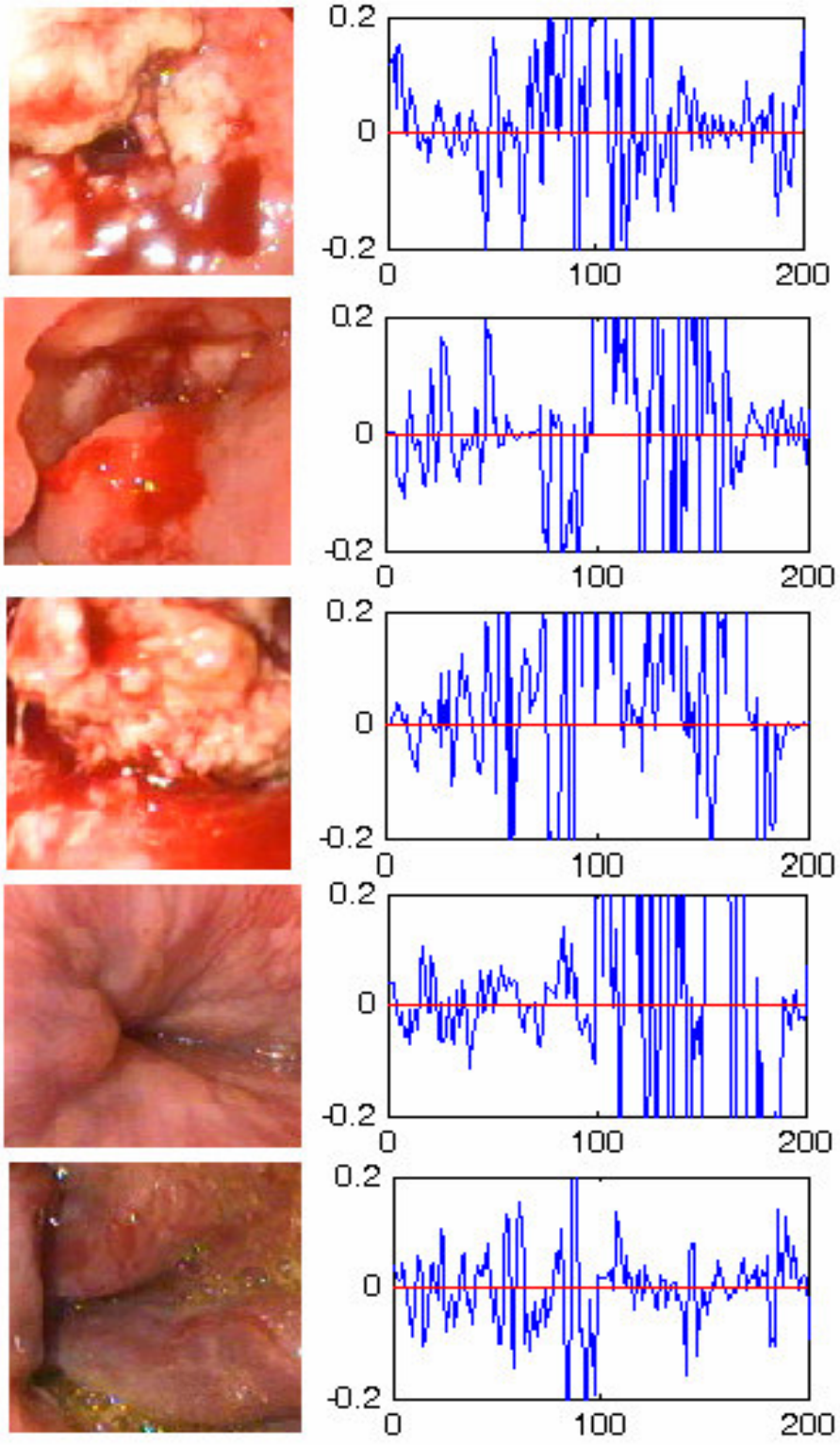

FIGURE 5: Curvature profile for Abnormal Images.

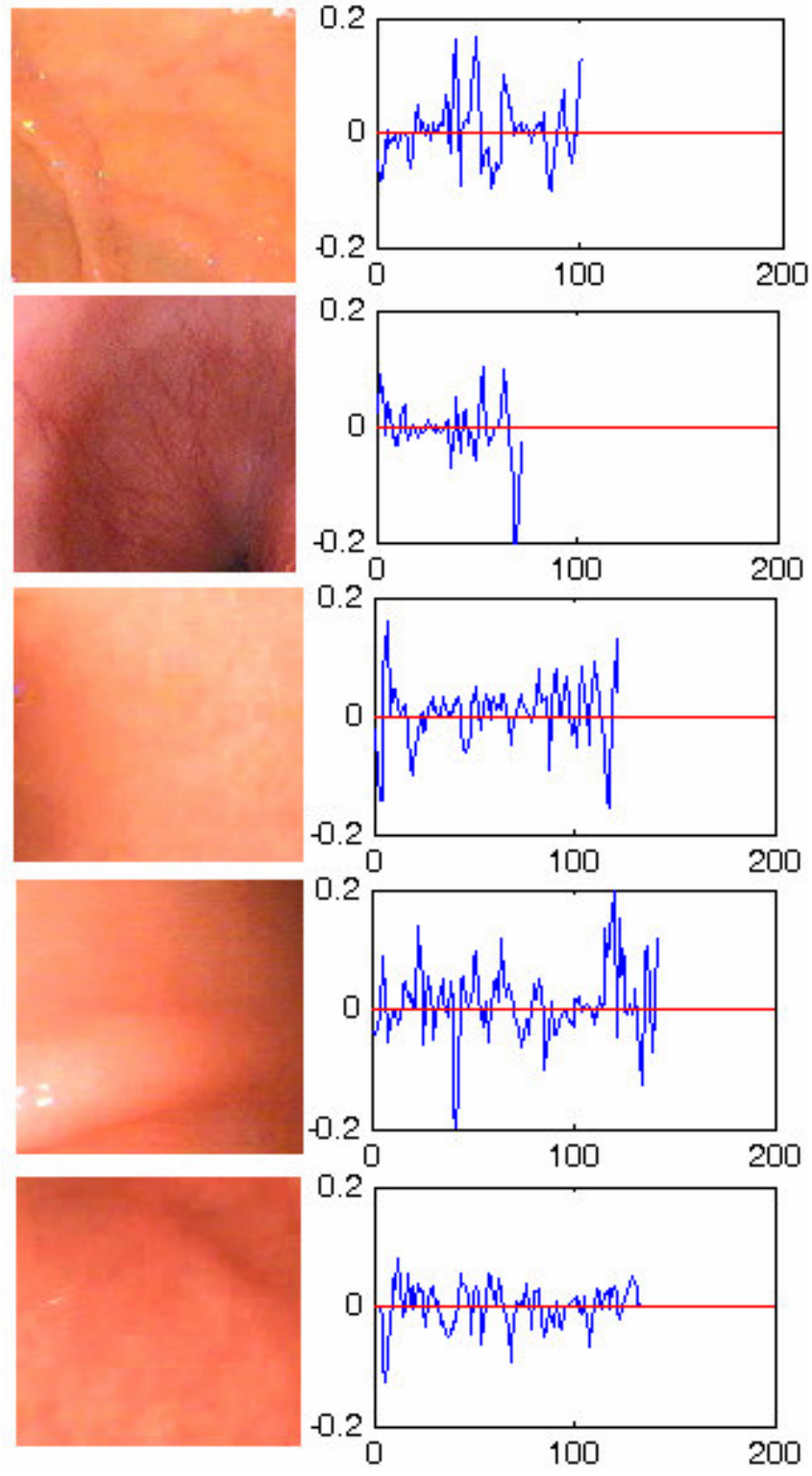

FIGURE 6: Curvature profile for Normal Images.

Abnormal Images			Normal Images		
Image ID	**Regions**	**Zero Crossings**	**Image ID**	**Regions**	**Zero Crossings**
Abn01	31	164	Nor01	5	89
Abn02	29	105	Nor02	9	29
Abn03	14	106	Nor03	4	69
Abn04	18	160	Nor04	9	81
Abn05	8	122	Nor05	2	53
Abn06	29	155	Nor06	4	78
Abn07	25	156	Nor07	9	48
Abn08	26	157	Nor08	5	53
Abn09	14	111	Nor09	5	70
Abn10	10	115	Nor10	2	69
Abn11	9	91	Nor11	2	40
Abn12	17	161	Nor12	4	89
Abn13	12	145	Nor13	3	50
Abn14	38	136	Nor14	2	38
Abn15	11	107	Nor15	2	72
Abn16	11	118	Nor16	2	70
Abn17	14	94	Nor17	6	64
Abn18	13	100	Nor18	2	42
Abn19	11	124	Nor19	9	143
Abn20	11	202	Nor20	3	62
Abn21	18	176	Nor21	5	57
Abn22	20	178	Nor22	2	36
Abn23	18	99	Nor23	8	96
Abn24	14	148	Nor24	6	87
Abn25	29	168	Nor25	4	59
Abn26	16	131	Nor26	4	51
Abn27	16	139	Nor27	4	74
Abn28	10	108	Nor28	2	78
Abn29	28	252	Nor29	3	60
Abn30	24	206	Nor30	3	66
Abn31	19	131	Nor31	3	66
Abn32	18	97	Nor32	4	51
Abn33	21	148	Nor33	2	29
Abn34	27	117	Nor34	7	141
Abn35	40	153	Nor35	2	34
Abn36	20	130	Nor36	3	59
Abn37	10	158	Nor37	2	83
Abn38	10	109	Nor38	2	54
Abn39	16	159	Nor39	5	70
Abn40	13	147	Nor40	4	71
Abn41	26	151	Nor41	7	156
Abn42	11	142	Nor42	2	67
Abn43	22	168	Nor43	3	53
Abn44	17	213	Nor44	2	48
Abn45	11	151	Nor45	4	138
Abn46	15	167	Nor46	4	27
Abn47	14	117	Nor47	5	128
Abn48	33	150	Nor48	3	61
Abn49	27	138	Nor49	3	56
Abn50	31	141	Nor50	5	71

TABLE 1: Number of Regions and Zero Crossings for Normal and Abnormal Images.

Table 1 show the number of regions obtained after the segmentation by the active contours without edges and total number of zero crossings for all the edges obtained in the segmented image. The results are shown for the 50 normal and 50 abnormal test images. In the results it can be seen that the proposed segmentation for the abnormal images generate large number of regions when compared to the normal images. We can notice that few normal images have generated large number of segments and zero crossings. It is due to the presence of noise such as lumen regions and bright spots generated by the reflection of light sources.

The following Table 2 shows the classification results using the nearest neighbor and K nearest neighbor classifiers.

Image Type	NN Classifier	KNN Classifier
Abnormal Images	96%	98%
Normal Images	90%	90%

TABLE 2: Classification Results.

6. CONCLUSION

The proposed segmentation method is based on the active contours without edges using Mumford-Shah [9] technique and it does not rely on the boundaries defined by the gradients. Also it starts with one initial curve and splits itself to detect the interior curves forming number of regions depending on the smoothness of the surface. The boundary curvature depends on the roughness of the image surface. It generates less number of zero crossings for the smooth normal images where as large number of zero crossings for relatively rough texture in abnormal images. Results obtained from the NN and KNN classifier are quite encouraging. The other features of endoscopic images such as color can be used in future to improve the classification results.

7. REFERENCES

[1] http://digestive.healthcentersonline.com/digestiveimagingtest/endoscopy.cfm

[2] P. Wang, S. M. Krishnan, C. Kugean, M.P. Tjoa, *"Classifiation of Endoscopic images based on Texture and Neural Network"*, In Proceedings of the 23rd Annual EMBS International Conference, October 25-28, Intanbul, Turkey

[3] S. M. Krishnan, X. Yang, K. L. Chan, S. Kumar, P. M. Y. Goh, *"Intestinal Abnormality Detection from Endoscopic Images"*, In Proceedings of 20th Annual International Conference of IEEE EMBS 98, Hongkong, 1998

[4] P.S.Hiremath, B.V.Dhandra, Ravindra Hegadi, G.G.Rajput, *"Abnormality detection in endoscopic images using color segmentation and curvature computation"*, In Proceedings of 11th International Conference on Neural Information Processing, ICONIP-2004, ISI, Calcutta, India, LNCS, ISBN-3-540-23931-6, Springer-Verlag, 2004

[5] P. S. Hiremath, B.V. Dhandra, Iranna Humnabad, Ravindra Hegadi, G.G. Rajput, *"Detection of esophageal Cancer (Necrosis) in the Endoscopic images using color image segmentation",* In Proceedings of second National Conference on Document Analysis and Recognition (NCDAR-2003), Mandya, India, 2003

[6] B.V.Dhandra, Ravindra Hegadi, *"Classification of Abnormal Endoscopic Images using Morphological Watershed Segmentation",* In Proceedings of International Conference on Cognition and Recognition (ICCR-2005), Mysore, India, 2005

[7] Tony F. Chan, Luminita A. Vese, *"Active Contours without Edges"*, IEEE Transactions on Image Processing, 10(2), 2001

[8] S. Osher, J. A. Sethian, *"Front propagating with curvature dependent speed: Algorithm based on Hamilton-Jacobi formulation"*, Journal of Computational Physics, 79:12-49, 1988

[9] D. Mumford, J. Shah, *"Optimal approximation by piecewise smooth functions and associated variational problems"*, Communications on Pure and Applied Mathematics, 42:577-685,1989

[10] Eric W. Weisstein, *"Jacobi Method, Technical Report"*

[11] V. Torre, T. A. Poggio, *"On Edge Detection*", IEEE Transactions on Pattern Analysis and Machine Intelligence, 8:147-163, 1986

[12] N. Ansari, K.W. Huang, *"Non-parametric Dominant Point Detection"*, Pattern Recognition, 24:849-862,1991